Intrathecal gene therapy rescues a model of demyelinating peripheral neuropathy

Alexia Kagiava[a], Irene Sargiannidou[a], George Theophilidis[b], Christos Karaiskos[a], Jan Richter[c], Stavros Bashiardes[c], Natasa Schiza[a], Marianna Nearchou[d], Christina Christodoulou[c], Steven S. Scherer[e], and Kleopas A. Kleopa[a,f,1]

[a]Neuroscience Laboratory, Cyprus School of Molecular Medicine, The Cyprus Institute of Neurology and Genetics, 1683 Nicosia, Cyprus; [b]Laboratory of Animal Physiology, Department of Zoology, School of Biology, Aristotle University of Thessaloniki, 54124 Thessaloniki, Greece; [c]Department of Molecular Virology, Cyprus School of Molecular Medicine, The Cyprus Institute of Neurology and Genetics, 1683 Nicosia, Cyprus; [d]Department of Molecular Pathology and Electron Microscopy, Cyprus School of Molecular Medicine, The Cyprus Institute of Neurology and Genetics, 1683 Nicosia, Cyprus; [e]Department of Neurology, The University of Pennsylvania, Philadelphia, PA 19104; and [f]Neurology Clinics, Cyprus School of Molecular Medicine, The Cyprus Institute of Neurology and Genetics, 1683 Nicosia, Cyprus

Inherited demyelinating peripheral neuropathies are progressive incurable diseases without effective treatment. To develop a gene therapy approach targeting myelinating Schwann cells that can be translatable, we delivered a lentiviral vector using a single lumbar intrathecal injection and a myelin-specific promoter. The human gene of interest, *GJB1*, which is mutated in X-linked Charcot–Marie–Tooth Disease (CMT1X), was delivered intrathecally into adult *Gjb1*-null mice, a genetically authentic model of CMT1X that develops a demyelinating peripheral neuropathy. We obtained widespread, stable, and cell-specific expression of connexin32 in up to 50% of Schwann cells in multiple lumbar spinal roots and peripheral nerves. Behavioral and electrophysiological analysis revealed significantly improved motor performance, quadriceps muscle contractility, and sciatic nerve conduction velocities. Furthermore, treated mice exhibited reduced numbers of demyelinated and remyelinated fibers and fewer inflammatory cells in lumbar motor roots, as well as in the femoral motor and sciatic nerves. This study demonstrates that a single intrathecal lentiviral gene delivery can lead to Schwann cell-specific expression in spinal roots extending to multiple peripheral nerves. This clinically relevant approach improves the phenotype of an inherited neuropathy mouse model and provides proof of principle for treating inherited demyelinating neuropathies.

demyelinating neuropathy | Charcot–Marie–Tooth disease | connexin32 | peripheral nerve | gene therapy

Inherited demyelinating neuropathies result from genetic defects in a variety of genes that are expressed by myelinating Schwann cells (1). These mutations are thought to cause demyelination in a cell-autonomous manner. Recessively inherited disorders cause loss of function, and dominantly inherited disorders cause haplotype insufficiency or toxic gain of function (2, 3). Achieving a therapeutic correction of these genetic defects requires either gene replacement or gene silencing approaches, ideally confined to myelinating Schwann cells (4).

Various techniques for gene delivery to peripheral nerves have been attempted, including adenoviral (AV) and adeno-associated viral (AAV) vectors and ubiquitous promoters (5). Intramuscular and direct intraneural injections help restrict expression to Schwann cells, but the duration of expression is typically limited. Lentiviral vectors produce sustained expression and have been injected intraneurally in crushed sciatic nerves to achieve retrograde transport and gene expression in motor neurons (6) and locally to transduce Schwann cells (7). None of the approaches published to date has provided a Schwann cell-specific gene delivery method to achieve widespread and stable expression.

We recently reported Schwann cell-specific expression driven by the rat myelin protein zero (*Mpz*) promoter of a neuropathy gene following intraneural lentiviral vector delivery, alleviating pathological changes in a model of X-linked Charcot–Marie–Tooth disease (CMT1X) (8). Expression was restricted to the

injected sciatic nerve, however, thus limiting its usefulness for clinical applications.

Here we report a gene delivery approach via a single lumbar intrathecal injection leading to stable Schwann cell gene expression in an unexpectedly widespread distribution—the lumbar spinal roots and along the entire length of the femoral and sciatic nerves. Using this approach to treat a mouse model of CMT1X resulted in significant behavioral, functional, and morphological improvement, providing an important advance toward treating inherited neuropathies.

Results

Establishment of Intrathecal Gene Delivery Targeting Schwann Cells.
The LV.*Mpz-Egfp* mock vector uses the rat *Mpz* promoter to drive expression of enhanced green fluorescent protein (EGFP) in myelinating Schwann cells (9) (*SI Appendix,* Fig. S1A). The vector was delivered intrathecally by a single injection at the L5-L6 intervertebral space (*SI Appendix,* Fig. S2) in 2-mo-old wild type (WT) mice. The expression of the reporter gene EGFP was examined by immunostaining and immunoblot analysis of multiple lumbar roots and peripheral nerves at 2, 8, and 16 wk postinjection. Widespread EGFP expression was detected in the perinuclear Schwann cell cytoplasm and sometimes also in the paranodal region of the myelin sheath in posterior/sensory and

Significance

Inherited demyelinating peripheral neuropathies are progressive incurable diseases caused by mutations in a variety of genes expressed by myelinating Schwann cells. A major challenge in developing effective gene therapy is to gain access to multiple nerves for cell-specific expression. Our study demonstrates for the first time, to our knowledge, that intrathecal injection of a lentiviral vector with a myelin-specific promoter can achieve targeted expression in adult myelinating Schwann cells in a widespread distribution throughout the peripheral nervous system. Furthermore, this translatable approach restored the expression of a neuropathy-associated gene and led to a phenotypic, functional, and pathological rescue of a neuropathy model. These results have important implications for further preclinical and clinical testing in this and other types of inherited demyelinating neuropathies.

anterior/motor lumbar roots; in the myelinated fibers entering the dorsal root ganglia (DRG); in femoral motor nerves; in proximal, middle, and distal parts of the sciatic nerve; as well as in intramuscular nerves of the quadriceps muscle, indicating spread through the roots to the peripheral nerves (Fig. 1 and *SI Appendix*, Figs. S1 *B* and *C* and S3).

EGFP expression was limited to myelinating Schwann cells and was not detected in any of the various cell types of the peripheral nervous system (PNS), including perineurial cells, neurons in the DRG or lumbar spinal cord, axons, endothelial cells, fibroblasts (*SI Appendix*, Fig. S4) or nonmyelinating Schwann cells (*SI Appendix*, Fig. S5). Expression rates (percentage of EGFP$^+$ Schwann cells) varied among areas, with the highest rates detected in the sciatic nerve (56.5 ± 3.5%), followed by the femoral motor nerve (48 ± 5.0%), anterior lumbar roots (42.5 ± 2.4%), DRG (39.3 ± 3.9%), and posterior lumbar roots (34.2 ± 2.8%). Similar ratios of EGFP-expressing Schwann cells were obtained from teased fiber preparations and from cross-cryosections of peripheral nerves (*SI Appendix*, Fig. S6). Expression rates increased over time from 2 wk to 16 wk postinjection ($P < 0.05$). The largest increase was detected in the sciatic nerve ($P < 0.01$) (Fig. 1*G* and *SI Appendix*, Table S1). Further analysis of genome vector copy numbers (VCN) in spinal roots and different sections of peripheral nerves confirmed the diffusion of the vector (Fig. 1*H*).

In contrast, no vector was detected systemically (*SI Appendix*, Table S2). EGFP expression in lumbar roots and sciatic nerves was confirmed by immunoblot analysis (Fig. 1*I*), and expression was not detected in corresponding tissues from control (noninjected) mice (*SI Appendix*, Fig. S7).

Virally Induced Expression of the Human *GJB1* Gene in *Gjb1*-Null Mice. These results motivated us to examine the efficacy of the LV.*Mpz-GJB1* full vector in *Gjb1*/Cx32 knockout (Cx32 KO) mice, which develop a progressive demyelinating neuropathy starting after age 3 mo (10, 11), providing an authentic model of CMT1X (12). This vector contains the human *GJB1* gene, which encodes connexin32 (Cx32), a gap junction protein found in the Schwann cell myelin sheath localized in the noncompact myelin areas, including paranodal loops and Schmidt–Lantermann incisures (13). We previously showed that transgenic expression of human Cx32 can rescue the phenotype in Cx32 KO mice (9), that most CMT1X-associated *GJB1* mutations cause a loss of Cx32 function (14), and that sciatic intraneural injection of this vector restores local Cx32 expression in this CMT1X model (8).

Thus, we performed lumbar intrathecal injections of LV.*Mpz-GJB1* into 2-mo-old Cx32 KO mice and then immunostained teased fibers from lumbar spinal roots and sciatic and femoral motor nerves at 4–6 wk postinjection. Cx32 immunoreactivity
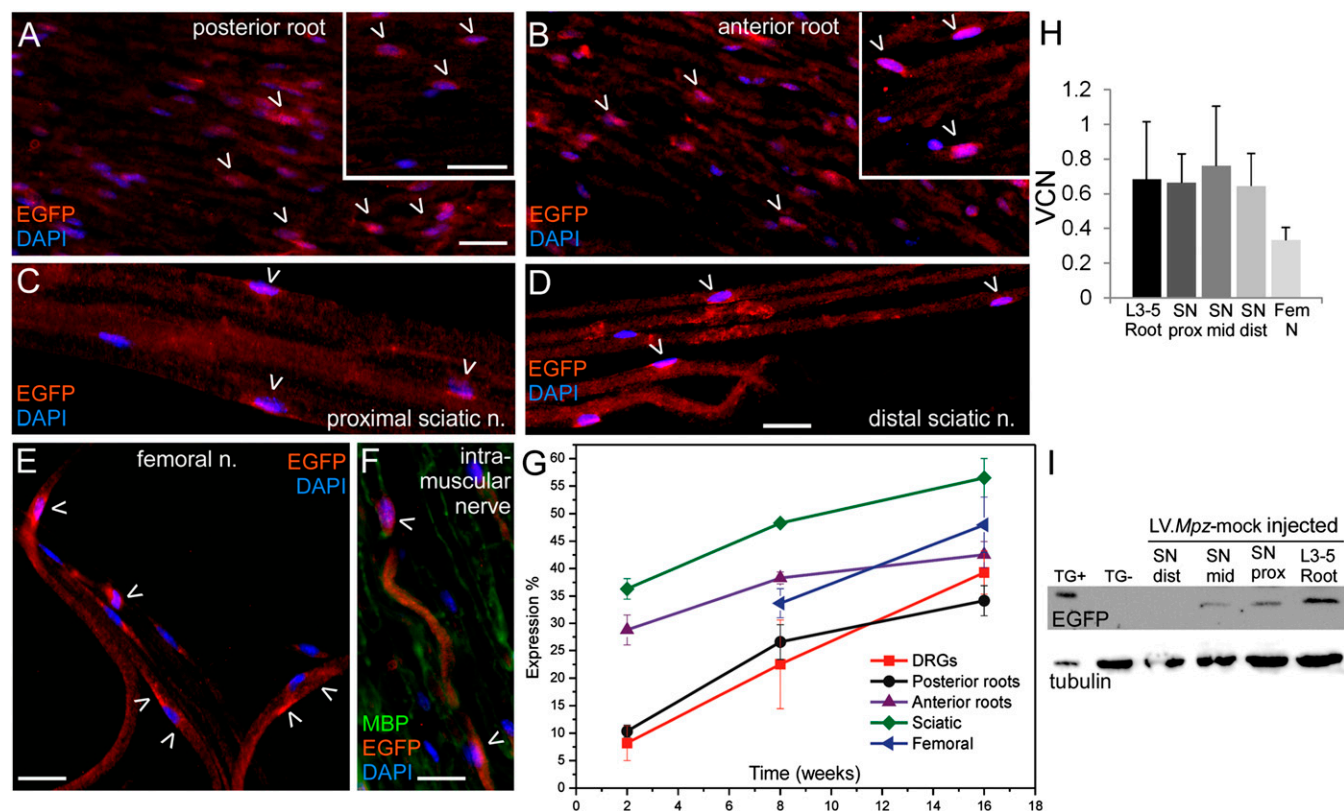

Fig. 1. Intrathecal lentiviral vector delivery and analysis of reporter gene expression. Immunostaining for EFGP (red) at 16 wk after injection of the LV.*Mpz* mock vector reveals EGFP expression in the perinuclear cytoplasm (open arrowheads) in a subset of Schwann cells in cryosections of posterior (*A*) and anterior (*B*) lumbar roots, in teased fibers from the proximal (*C*) and distal (*D*) sciatic nerve and from the femoral motor nerve (*E*), as well as in intramuscular nerves from quadriceps muscle sections (*F*). (*A* and *B*, *Insets*) Higher-magnification views of Schwann cells. Schwann cell nuclei are stained with DAPI (blue) throughout, and intramuscular nerves in *F* are double-labeled with myelin basic protein (green). (Scale bars: 10 μm.) (*G*) Quantification of EGFP-expressing Schwann cells at 2, 8, and 16 wk postinjection ($n = 3$ mice per time point) in DRGs, anterior and posterior lumbar roots, sciatic nerves, and femoral motor nerves shows increasing expression over time (data in *SI Appendix*, Table S1). (*H*) Measurements of genome VCN in lumbar roots (L3-5 root), proximal (prox), middle (mid), and distal (dist) parts of the sciatic nerve (SN), as well as the femoral nerve (Fem N), from $n = 2–5$ mice at 4 wk after intrathecal injection as indicated, confirm diffusion of the vector to the peripheral nerves and are consistent with the expression rates (no significant differences between tissues examined; data in *SI Appendix*, Table S2). (*I*) Immunoblot analysis confirms EGFP expression in different tissues from injected mice as indicated as opposed to a noninjected mouse nerve (TG−). TG+ is a positive control nerve sample from a mouse transgenically expressing EGFP. β-Tubulin served as a loading control.
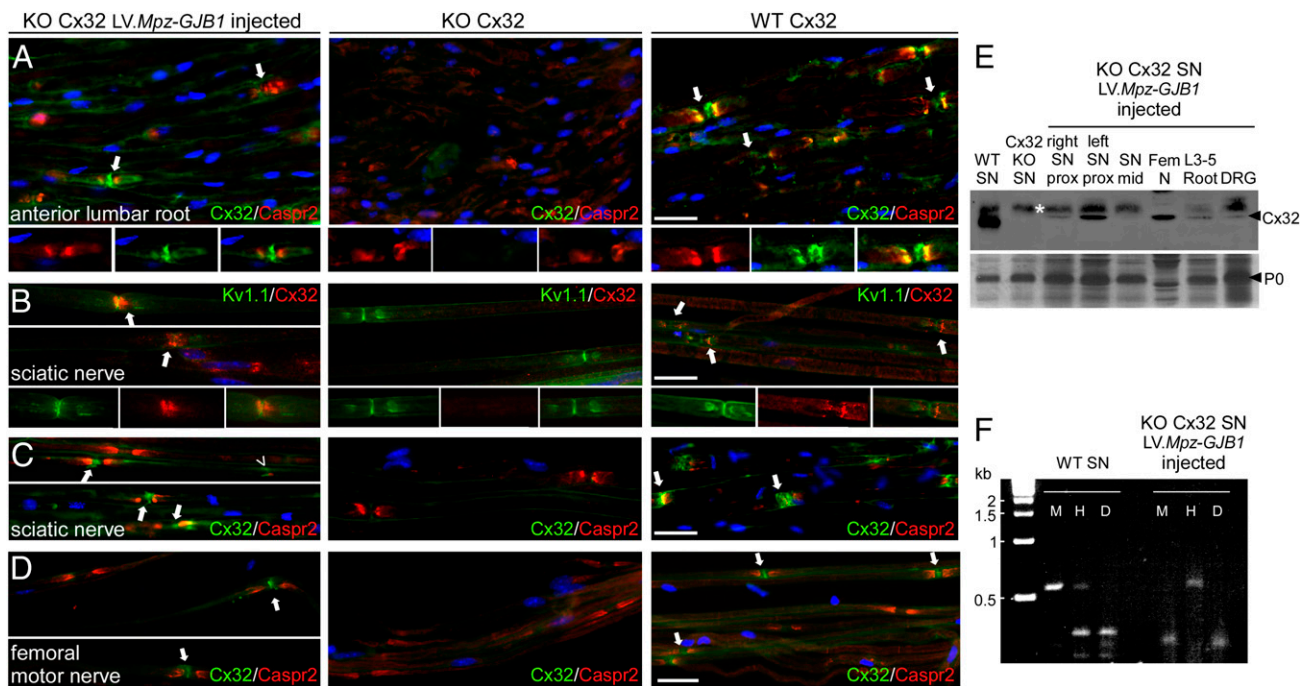
Fig. 2. Widespread expression of Cx32 in Schwann cells throughout the PNS following intrathecal vector delivery. Images of anterior lumbar root longitudinal sections (*A*) and teased fibers from sciatic (*B* and *C*) and femoral motor (*D*) nerves from Cx32 KO mice injected with the LV.*Mpz-GJB1* vector (*Left*; n = 3), noninjected Cx32 KO mice (*Middle*), and control WT mice (*Right*) as indicated, immunostained for Cx32 (green in *A*, *C*, and *D* and red in *B*) and either Caspr2 (red in *A*, *C*, and *D*) or Kv1.1 (green in *B*). Cell nuclei are stained with DAPI (blue). Cx32-immunoreactivity is present in paranodal myelin areas (arrows) surrounding juxtaparanodal Caspr2 or Kv1.1 immunoreactivity in injected KO mice, similar to WT mice, but absent from noninjected Cx32 KO lumbar roots and nerves. The images in *B*, *Left* are noncontiguous, and those in *C* and *D* are taken from two different photographs. (Scale bars: 10 μm.) (*E*) Immunoblot detection of Cx32 in different Cx32 KO tissues as indicated at 6 wk after LV.*Mpz-GJB1* injection shows a specific band of variable intensity in all samples, which is also present in a WT nerve (positive control), but absent from a noninjected Cx32 KO nerve. *Indicates a nonspecific band. P0 bands on Coomassie blue-stained gel are shown underneath as a loading control. (*F*) RT-PCR and digestion by MscI (M; cuts the human *GJB1* cDNA) or HhaI (H; cuts the mouse *Gjb1* cDNA), or with both (D; "double-cut") shows M-digested human *GJB1* cDNA only in the LV.*Mpz-GJB1*-injected Cx32 KO nerve and H-digested mouse *Gjb1* cDNA only in the WT nerve.

was detected in all tissues and was correctly localized in paranodal myelin loops, as indicated by double staining with antibodies to Caspr2 or Kv1.1, which label the juxtaparanodal domains of myelinated axons (Fig. 2 *A–D* and *SI Appendix*, Figs. S8 and S9). Virally driven Cx32 was localized similarly to endogenous Cx32 in WT mice, whereas Cx32-immunoreactivity was absent from lumbar roots of noninjected Cx32 KO mice. We also detected exogenous Cx32 in the femoral motor (Fig. 2*D*) and even in the trigeminal nerves (*SI Appendix*, Fig. S10) of injected Cx32 KO mice, indicating spread of the vector through the cerebrospinal fluid (CSF), with correct localization of Cx32 and no Cx32 immunoreactivity in noninjected Cx32 KO nerve.

We confirmed the expression of Cx32 by immunoblot analysis and RT-PCR. Cx32 was detected in lysates from Cx32 KO mice intrathecally injected with LV.*Mpz-GJB1* (Fig. 2*E*), although the levels were lower than the endogenous expression in WT mice. Furthermore, we amplified RNA extracted from sciatic nerve tissues into cDNA using primers that are identical in both human and mouse Cx32 mRNA, resulting in a 553-bp product. Digestion with restriction enzymes specific for human or mouse Cx32 transcript (14) showed that sciatic nerves of intrathecally injected Cx32 KO mice contained only the human Cx32 transcript, whereas control WT mice contained only the mouse Cx32 transcript (Fig. 2*F*).

To determine whether intrathecal vector injection causes an inflammatory response, we immunostained lumbar spinal roots from injected Cx32 KO mice with lymphocyte and macrophage markers at 6 wk after vector delivery. This analysis revealed no evidence of increased inflammatory cell infiltration in injected

compared with WT or noninjected 3-mo-old Cx32 KO mice (*SI Appendix*, Fig. S11). Furthermore, there was no evidence of a disrupted blood–spinal cord barrier as a result of the intrathecal injection (*SI Appendix*, Fig. S12).

Intrathecal Gene Therapy Trial in 2-Mo-Old Cx32 KO Mice. Having established that intrathecal gene delivery leads to widespread expression of Cx32 in Schwann cells, we proceeded with a treatment trial. We performed intrathecal injection of the LV.*Mpz-GJB1* vector or LV.*Mpz-Egfp* mock vector into randomized littermate groups of 2-mo-old Cx32 KO mice (before the onset of demyelination) (10, 11, 15). The mice were examined by behavioral analysis to assess motor function at age 4 and 8 mo, as well as by electrophysiological and pathological analysis at age 8 mo. All behavioral and physiological observations, as well as morphological analyses, were done by observers blinded to the treatment condition.

Improvement of Motor Performance in Treated Cx32 KO Mice. Rotarod analysis at 4 mo showed that at a speed of 20 rpm, the fully treated mice (n = 6) remained on the rotarod significantly longer than the mock-injected mice (n = 12) (mean, 444 ± 99 s vs. 90.7 ± 23 s; $P < 0.001$) (Fig. 3*A*). Likewise, at 32 rpm, the fully treated mice remained on the rotarod significantly longer than the mock-treated mice (mean, 160 ± 54 s vs. 21.8 ± 8.5 s; $P < 0.05$). Similar results were obtained at age 8 mo; at 20 rpm, the fully treated mice (n = 18) remained on the rotarod for a mean of 394 ± 44 s, compared with for 90.5 ± 18 s for the mock-treated mice (n = 20) ($P < 0.05$); at 32 rpm, mean times on the
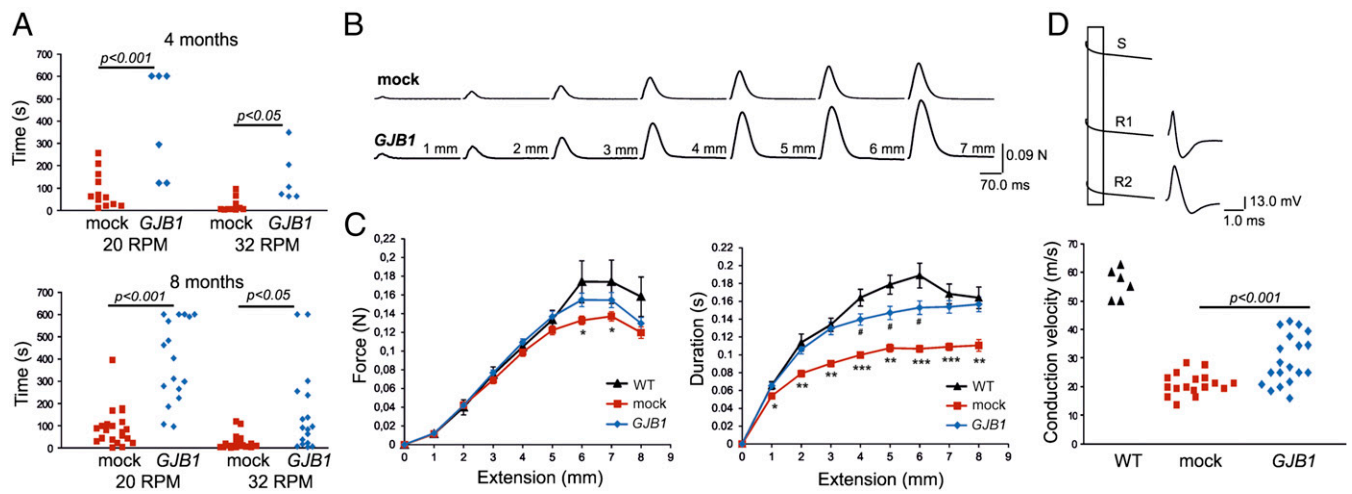
Kagiava et al.

Fig. 3. Behavioral and physiological improvement in intrathecally treated Cx32 KO mice. (*A*) Results from behavioral analysis showing improved rotarod motor performance in LV.*Mpz-GJB1*-injected (*GJB1*) Cx32 KO mice (*n* = 6 for 4 mo; *n* = 18 for 8 mo) compared with mock-treated (mock) (*n* = 12 for 4 mo; *n* = 20 for 8 mo) at both 4 mo (*Upper*) and 8 mo (*Lower*) at the two speeds tested. (*B*) Representative in situ recordings of the force of the quadriceps muscle contraction from mock-treated mice (*Upper*) and fully treated mice (*Lower*) showing increased force and duration of the muscle contraction in the fully treated mice at different extensions (indicated in millimeters). (*C*) (*Left*) Force of quadriceps muscle contraction is increased in the fully treated mice (*GJB1*; *n* = 10) at 8 mo compared with the mock-treated mice (mock; *n* = 9), showing no significant difference from the force recorded from WT mice (WT; *n* = 6). (*Right*) Duration of the contraction is also increased in the *GJB1*-treated mice compared with the mock-treated mice, almost reaching the values of the WT mice. *Significant differences between the fully treated and mock-treated mice; #significant differences between the fully treated and WT mice (unpaired *t* test). Values represent mean ± SEM. (*D*) (*Upper*) Ex vivo sciatic nerve preparation for the measurement of nerve CV. Hook electrodes were used for stimulating (S) and recording (R1, R2). Compound action potentials were recorded from two different parts of the nerve for CV calculation. (*Lower*) Quantification of sciatic CV shows increased CV in the *GJB1*-treated mice (*n* = 11) compared with the mock-treated mice (*n* = 9), but not reaching the normal values of WT mice (*n* = 6).

rotarod were 160 ± 46 s for the fully treated mice and 25.4 ± 7.1 s for the mock-treated mice ($P < 0.05$).

Hindlimb grip analysis showed a nonsignificant trend for higher force values generated by fully treated mice at 4 and 8 mo ($P > 0.05$). At 4 mo, the fully treated mice (*n* = 6) generated a mean force of 119 ± 17 g, compared with 92.4 ± 15.2 g in the mock-treated mice (*n* = 12); at 8 mo, these values were 123 ± 16 g (*n* = 18) and 98.6 ± 13 g (*n* = 20), respectively. Interestingly, foot grip force values were not significantly different between WT and Cx32 KO mice, indicating that this is not a discriminating test for this model (*SI Appendix*, Fig. S13). Finally, the mock-treated and fully treated mice showed similar performance in the foot slip test at age 4 and 8 mo, which was again similar to that of WT mice.

Improvement of Muscle Contractility in Treated 8-Mo-Old Cx32 KO Mice. We analyzed quadriceps muscle contraction after stimulation of the femoral motor nerve in situ using recordings like those presented in Fig. 3*B*. Both the force and the duration of contraction were improved in the fully treated mice compared with the mock-treated mice ($P < 0.05$), but were still lower than the values in the WT mice (Fig. 3*C*). The highest mean values were observed at a 6-mm extension in all cases, reaching 0.17 ± 0.02 N in the WT mice (*n* = 12 muscles, *n* = 6 mice), 0.13 ± 0.00 in the mock-treated mice (*n* = 18 muscles, *n* = 9 mice), and 0.15 ± 0.01 in the fully treated mice (*n* = 20 muscles, *n* = 10 mice) ($P < 0.05$). The mean duration of quadriceps contraction at a 6-mm extension reached 157 ± 8.2 ms in the fully treated mice and 111 ± 6.5 ms in the mock-treated mice ($P < 0.05$), whereas in the WT mice, the longest duration was 189 ± 14 ms. Muscle residual force during extension was increased by 20% in the fully treated mice (0.20 ± 0.01 N) compared with the mock-treated mice (0.16 ± 0.01 N).

Improvement of Sciatic Nerve Conduction Velocity in Treated 8-Mo-Old Cx32 KO Mice. Using the ex vivo setup presented in Fig. 3*D*, we determined the conduction velocity (CV) of sciatic nerves. The

mean CV in the fully treated Cx32 KO mice (29.3 ± 1.8 m/s; *n* = 22 nerves, *n* = 11 mice) was significantly faster than that in the mock-treated mice (21.1 ± 0.93 m/s; *n* = 18 nerves, *n* = 9 mice) ($P < 0.05$), but slower than that in the WT mice (55.9 ± 2.1 m/s; *n* = 6 nerves, *n* = 3 mice). The amplitude of the compound action potential (CAP), indicating nerve vitality, remained constant after monitoring velocity for more than 20 h in all groups.

Improved Pathology in Spinal Roots and Peripheral Nerves of Intrathecally Treated Cx32 KO Mice. Transverse, semithin sections of lumbar spinal cord with attached anterior and posterior roots, as well as femoral motor and midsciatic nerves, were prepared from 8-mo-old fully treated mice (*n* = 8) and mock-treated littermates (*n* = 8). Morphometric analysis in then semithin sections was performed by an observer who was blinded to the treatment condition. Multiple roots, as well as bilateral nerves when available, were examined, and results were averaged per mouse. The number of abnormally myelinated fibers, including demyelinated and remyelinated fibers, was counted and their proportion of the total number of fibers calculated (9, 14). Foamy macrophages were also counted (8), and their numbers per 1,000 myelinated fibers were compared (to account for variations in root and nerve size).

The ratios of abnormally myelinated fibers and foamy macrophages in the lumbar roots and peripheral nerves were significantly lower in the fully treated mice compared with the mock-treated mice (Figs. 4 and 5 and *SI Appendix*, Table S3). As expected, the highest proportion of abnormally myelinated fibers was found in the anterior (motor) lumbar roots and femoral motor nerves of mock-treated mice, in keeping with previous observations that neuropathy in Cx32 KO mice affects mainly the motor fibers (10, 11). In anterior lumbar spinal roots, the ratio of abnormal fibers was 0.054 ± 0.018 in the fully treated mice, compared with 0.159 ± 0.029 in the mock-treated mice ($P = 0.00094$, Mann–Whitney *U* test). Likewise, macrophage numbers in the anterior roots were lower in the fully treated mice (1.30 ± 1.8/1,000 fibers vs. 9.89 ± 2.5/1,000 fibers; $P = 0.00094$) (Fig. 4 *A* and *B*).
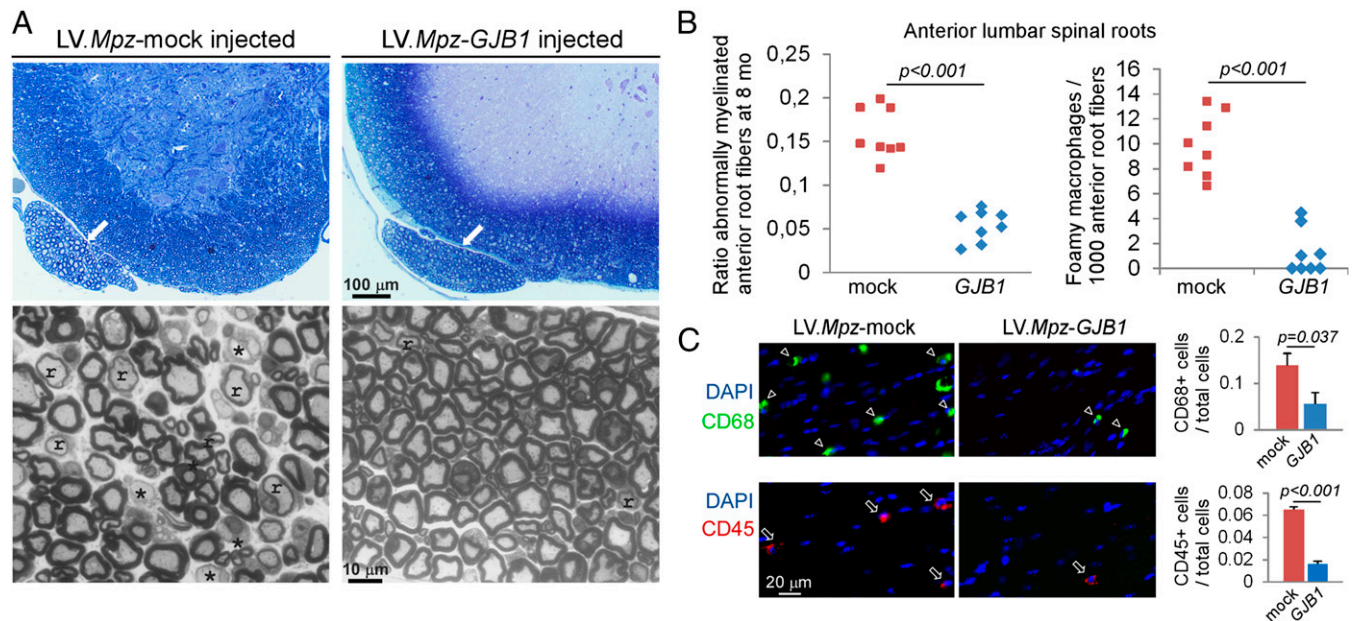
Fig. 4. Improvement of anterior lumbar spinal root demyelination and inflammation in 8-mo-old Cx32 KO mice following intrathecal gene therapy with the LV.*Mpz-GJB1* vector. (*A*) Representative images of semithin sections of anterior lumbar spinal roots attached to the spinal cord (arrows) at low magnification (*Upper*) and higher magnification (*Lower*) from mock-injected mice (*Left*) and LV.*Mpz-GJB1*-injected mice (*Right*) show improved myelination in the latter, with fewer demyelinated (*) or remyelinated (r) fibers. (*B*) Quantification of the ratios of abnormally myelinated fibers in multiple roots ($n = 8$ mice per group) confirms significant improvement, as well as a significant reduction in foamy macrophage numbers in the fully treated mice (*GJB1*) compared with the mock-treated mice (mock) (data in *SI Appendix*, Table S3). (*C*) Immunostaining of longitudinal lumbar spinal root sections with macrophage marker CD68 (green) or lymphocyte marker CD45 (red), as indicated (counterstaining with nuclear marker DAPI, blue), shows reduced numbers of inflammatory cells in roots from the fully treated mice. This is confirmed by quantifying the ratios of CD68^{+}/total cells ($n = 13$ roots from two fully treated mice and 16 roots from three mock-treated mice, a total of 3,433 cells counted) and of CD45^{+}/total cells ($n = 8$ roots from two fully treated mice and 14 roots from three mock-treated mice, a total of 2,139 cells counted) (Mann–Whitney *U* test).

Posterior lumbar roots showed overall minimal pathology even in the mock-treated mice, which improved in the fully treated mice.

Semithin sections of femoral motor nerve branches showed significant improvement in all pathological parameters in the fully treated mice, including the ratio of abnormal fibers (0.252 ± 0.037 in the mock-treated mice vs. 0.084 ± 0.050 in the fully treated mice; $P = 0.00094$) and the number of macrophages/1,000 fibers (7.26 ± 2.2 in mock-treated vs. 1.85 ± 1.3 in fully treated; $P = 0.00094$) (Fig. 5 *A* and *B*). Improvement was also observed in the sciatic nerves, with a ratio of abnormal fibers of 0.109 ± 0.013 in the mock-treated mice vs. 0.050 ± 0.013 in the fully treated mice ($P = 0.00094$) and macrophage numbers of 5.41 ± 1.4/1,000 fibers in mock-treated mice vs. 2.15 ± 1.0 in fully treated ($P = 0.00138$) (Fig. 5*C* and *SI Appendix*, Fig. S14).

To further examine the effect of treatment on inflammation, a well-characterized feature of Cx32 KO mice (16, 17), we also immunostained cryosections of lumbar roots and sciatic nerves from 8-mo-old mock-treated ($n = 4$) and fully treated ($n = 4$) mice with inflammatory cell markers. This analysis revealed lower numbers of CD68^{+} macrophages, CD3^{+} T lymphocytes, and CD45^{+} leukocytes in anterior spinal roots (Fig. 4*C*) and midsciatic nerves (*SI Appendix*, Fig. S15) in the fully treated mice compared with the mock-treated mice.

Discussion

In this study we describe a method for targeted gene delivery to myelinating cells of the PNS, involving intrathecal injection of a lentiviral vector driven by a myelin-specific promoter. Using this method, we achieved long-lasting and widespread expression of a reporter gene and a neuropathy-associated gene in multiple spinal roots and peripheral nerves, as well as rescue of the peripheral neuropathy phenotype in Cx32 KO mice, a model of CMT1X.

Previously attempted intraneural gene delivery using the same vector resulted in expression restricted to the injected sciatic nerve (8), whereas the intrathecal approach described here led to similar Schwann cell expression rates in sciatic nerves, but also achieved expression in multiple other peripheral nerves and spinal roots. This represents a major breakthrough, given that intrathecal injection is less invasive than other delivery methods and is routinely used in clinical practice for drug administration to treat pain, spasticity, and cancer.

Multiple spinal roots were labeled with this approach, presumably because they do not have a perineurial barrier, giving the virus access to the endoneurium of the spinal nerves. The extent of labeling in the sciatic and femoral nerves was unprecedented, most likely resulting from diffusion of the virus from the CSF to the endoneurium of the roots, spinal lumbosacral plexus, and peripheral nerves derived from them. The epineurial connective tissue layers merge with the dura matter at the central ends of peripheral nerves (18), providing continuity of the subarachnoid and endoneurial space (19) and allowing CSF to enter the endoneurial fluid. Diffusion of molecules injected into the midsciatic nerve has been shown up to 10 mm proximal and distal to the injection site, consistent with the flow of endoneurial fluid (20, 21). The higher pressure in the intrathecal CSF space (~10 mm Hg) compared with endoneural pressure in peripheral nerves (1–2 mm Hg) and DRG (3–5 mm Hg) supports the diffusion of particles from subarachnoid space into the peripheral nerves (22). In addition, expression in Schwann cells of the trigeminal nerve also indicates that viral infection following L5-6 intrathecal delivery is not confined to the lumbar roots, but may be widespread along the neuraxis following diffusion through the CSF.

Intrathecal injection has been previously used for gene delivery using AAV (23–27) and lentiviral vectors (28), and even
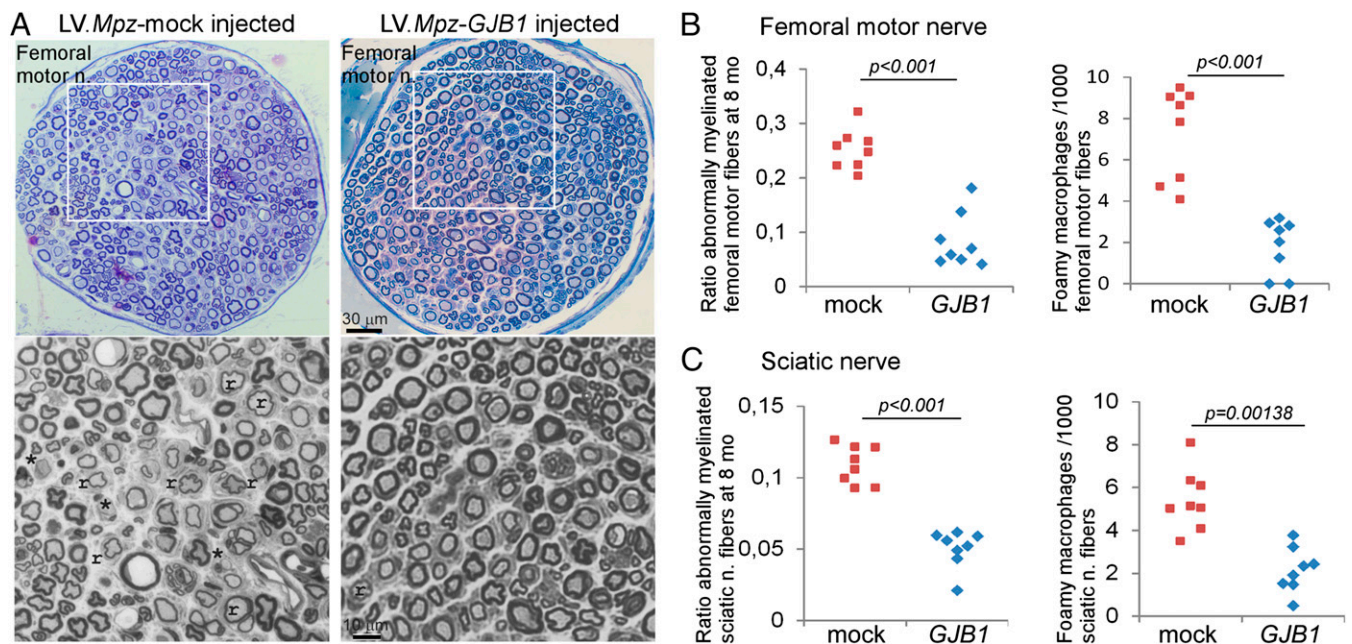
Kagiava et al.

NEUROSCIENCE

www.manaraa.com

Fig. 5. Improvement of demyelination and inflammation in femoral motor nerve branches and midsciatic nerves of 8-mo-old Cx32 KO mice following intrathecal gene therapy. (*A*) Overview of femoral motor nerve semithin sections (*Upper*) and higher-magnification images (*Lower*) shows improvement of demyelinating pathology in the LV.*Mpz-GJB1*-injected mice (*Right*) with fewer demyelinated (*) or remyelinated (r) fibers. (*B* and *C*) Quantification of the ratios of abnormally myelinated fibers in femoral motor nerves (*B*) and midsciatic nerves (*C*) (*n* = 8 mice per group) confirms significant improvement, as well as a significant reduction in foamy macrophage numbers in the fully treated mice (*GJB1*) compared with the mock-treated mice (mock) (Mann–Whitney *U* test; data in SI Appendix, Table S3).

without using viral vectors (29), to provide gene knockdown or gene silencing using shRNA or siRNA (30, 31), as well as in regeneration strategies using neural precursor cells (32). However, none of those previous studies focused specifically on myelinating Schwann cells, because ubiquitous promoters were used. Widespread expression was reported in some cases after AAV injection from the spinal cord to the brain in both adults and neonates (26, 33), and even after AAV9 injection in large animal models (27, 34). This is the first demonstration, to our knowledge, of a successful intrathecal approach to treating peripheral neuropathy by delivering a myelin-related gene and achieving widespread Schwann cell-specific expression.

Our approach resulted in restricted gene expression to Schwann cells throughout the PNS for at least 4 mo after a single injection, owing to use of the myelin-specific *Mpz* promoter. Although gene expression was found in the sciatic nerve after AAV vector delivery into the DRG, this was mainly in axons and DRG, and not in Schwann cells as in our study (23). Cell specificity is crucial for exogenous expression of neuropathy-associated genes such as Cx32, given that inherited demyelinating neuropathies result mostly from cell-autonomous loss of function in Schwann cells (35, 36).

Intrathecal gene delivery proved to be safe without any immunologic responses or spinal cord or root injury. This is in keeping with our previous observations following intraneural delivery of the same vector (8) or with preclinical (37, 38) and clinical (39) applications of similar lentiviral vectors. Rarely reported inflammatory responses (26) were attributed to the reporter gene and not to the intrathecal method of gene delivery or to the vector type.

Using a well-studied model of CMT1X, we demonstrate a significant benefit of intrathecal gene therapy for the peripheral neuropathy, leading to both morphological and functional improvement. Cx32 KO mice develop a progressive demyelinating, predominantly motor neuropathy after age 3 mo, with robust pathological findings in motor roots and nerves but relatively
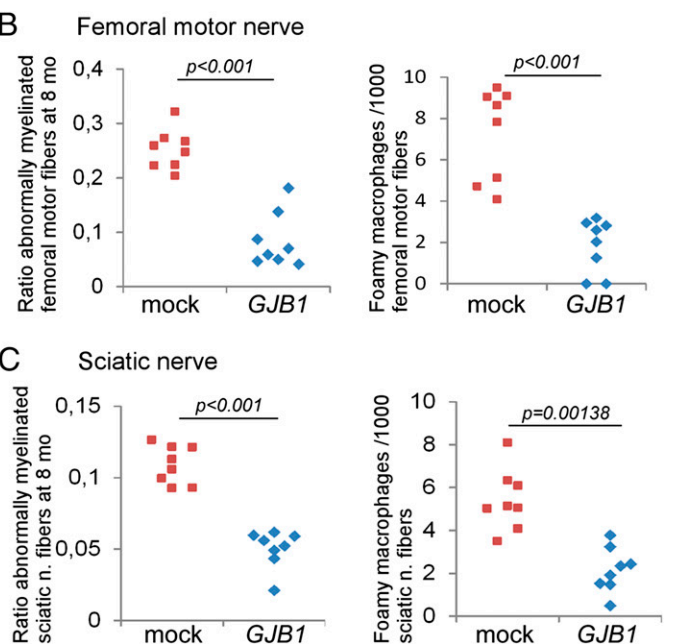
minimal, if any, behavioral and electrophysiological deficits (10, 11, 14). Our morphological analysis showed a clear reduction of demyelination and inflammation at age 8 mo following intrathecal gene therapy. As expected, this improvement was most pronounced in motor nerves and roots, whereas in sciatic nerves it was comparable to the approximate 50% improvement achieved with direct intraneural injection (8). This is consistent with the expression ratios of approximately 50% in Schwann cells, as well as the VCN results throughout the PNS tissues examined, and indicates that even partial expression may have therapeutic effects in future applications.

Pathological improvement was correlated with improved motor performance, as demonstrated by our rotarod analysis at both 4 and 8 mo of age. Other motor behavioral tests failed to show significant improvement, likely because even untreated Cx32 KO mice do not differ significantly from WT mice, at least at the ages examined here. Nevertheless, significant electrophysiological improvements in femoral motor-quadriceps muscle performance and ex vivo sciatic nerve CV provided a clear indication that intrathecally delivered human Cx32 is not only widely expressed and correctly localized, but also leads to functional rescue in this neuropathy model. This functional improvement did not reach WT levels, however, indicating the possible need for further increases in the number of infected Schwann cells and perhaps Cx32 expression level to achieve complete recovery.

In summary, we report a minimally invasive, clinically translatable method for gene delivery using a single lumbar intrathecal injection that provides long-lasting and widespread gene expression targeting the myelinating cells of the PNS. We also demonstrate a significant therapeutic benefit with this gene delivery method in a model of CMT1X inherited neuropathy. This approach is also relevant for other demyelinating neuropathies resulting from loss-of-function mechanisms and merits further study for clinical applications.

Kagiava et al.

Materials and Methods

Cloning and Production of Lentiviral Vectors. Cloning of the lentiviral vectors (*SI Appendix*, Fig. S1A), as well as methods of vector production and titration, have been described elsewhere (8); details are provided in *SI Appendix, Materials and Methods*.

Animals. Unless noted otherwise, the intrathecal gene delivery experiments were conducted using 2-mo-old WT C57BL/6 or *Gjb1*-null/Cx32 KO (C57BL/6_129) mice weighing 20–25 g, obtained from the European Mouse Mutant Archive, originally generated by Prof. Klaus Willecke (University of Bonn). All experimental procedures were conducted in accordance with animal care protocols approved by the Cyprus Government's Chief Veterinary Officer (project license CY/EXP/PR.L2/2012) according to national law, which is harmonized with EU guidelines (EC Directive 86/609/EEC).

Intrathecal Vector Delivery. Following a small skin incision along the lower lumbar spine level to visualize the spine, the lentiviral vector was delivered into the L5-L6 intervertebral space of anesthetized mice (*SI Appendix*, Fig. S2). A 100-μL Hamilton syringe connected to a 30-gauge needle was used to inject 30 μL of lentiviral stock containing an estimated 3.6×10^{11} (full vector) and 4×10^{12} (mock vector) viral particles/mL. A flick of the tail was considered indicative of successful intrathecal administration. Animals were euthanized, and dissected tissues were analyzed by immunohistochemistry, immunoblotting, and RNA expression at 4–6 wk postinjection.

VCN Determination. Genomic DNA was extracted from different PNS tissues (i.e., lumbar roots, proximal, middle and distal sciatic nerve, and femoral nerve) of mice at 1 mo after intrathecal vector delivery using the Invitrogen iPrep PureLink gDNA Kit (Thermo Fisher Scientific). The extracted DNA was analyzed for yield and purity using a Nanodrop 1000 spectrophotometer. Approximately 20 ng of DNA was used as template for two real-time PCR assays on an Applied Biosystems 7500 Real-Time PCR System involving 45 cycles of 15 s at 95 °C and 60 s at 60 °C. PCBP2-specific primers/probe targeting the mouse genome (40, 41) and eGFP-specific primers/probe targeting the EGFP gene, which is contained in the transgene, were used. Standard curves were created by serial dilution of quantified mouse genomic DNA, as well as quantified plasmid DNA containing the transgene cassette. The average VCN per cell was calculated as the total VCN divided by the total cell number. For the analysis of mouse serum for the presence of viral vectors, RNA was extracted from 60 μL of serum from mice ($n = 7$) at 1 mo after intrathecal vector injection using the iPrep Purelink Virus Kit (Thermo Fisher Scientific) and eluted in 50 μL. A one-step real-time RT-PCR assay, as described above for titration of the lentiviral vectors, was used to determine the presence or absence of lentiviral particles in the mouse circulation.

Intrathecal Gene Therapy Trial. The gene therapy trial was conducted using two groups ($n = 20$ per group) of Cx32 KO mice. Animals were treated at age 2 mo, before nerve pathology develops. Littermate mice were randomized to receipt of either LV.*Mpz-GJB1* (full) treatment or LV.*Mpz-Egfp* (mock treatment, as a control group) and assigned a coding number for further identification. Mice were evaluated by clinical testing at age 4 mo and 8 mo by a blinded examiner and used at age 8 mo in the electrophysiology experiments ($n = 8$ per group) or quantitative morphometric analysis of semithin sections ($n = 8$ per group) or frozen immunostained tissues ($n = 4$–5 per group). Analysis of physiological and morphological results was performed blinded to the treatment condition.

Rotarod Testing. Motor balance and coordination was determined as described previously (42) using an accelerating rotarod apparatus (Ugo Basile). LV.*Mpz-GJB1*- and LV.*Mpz-Egfp*-treated mice were tested at age 4 mo and 8 mo. Training of animals consisted of three trials per day with 15-min rest period between trials, for 3 consecutive days. The LV.*Mpz-GJB1*- and LV.*Mpz-Egfp*-treated mice were placed on the rod, and the speed was gradually increased from 4 to 40 rpm. The trial lasted until the mouse fell from the rod or after the mouse remained on the rod for 600 s and was then removed. Testing was performed on the fourth day using two different speeds, 20 and 32 rpm. Latency to fall was calculated for each speed. Details of the grip strength and foot slip tests (43) are provided in *SI Appendix, Materials and Methods*.

Quadriceps Muscle Contractility Study. In situ assessment of lumbar root and femoral motor axon function was done by measuring the properties of the muscle contraction of the quadriceps muscle innervated by the femoral nerve in an anesthetized mouse according to institutionally approved protocols,

using a modified method described by Pratt and Lovering (44). After the motor part of the femoral nerve was exposed, a stimulating hook electrode was used to stimulate the motor branch of the femoral nerve at 1 Hz using a constant-current stimulator (DS3; Digitimer) at 5–6 mA and a 200-μs pulse duration. Muscle contractions of the partially exposed quadriceps muscle were recorded with a force displacement transducer (FT03; Grass Technologies), which was attached to the muscle with a silk suture. The transducer was attached on a micromanipulator, and for the experiment the muscle was extended 1 mm each time until the muscle contraction reached its maximum value. The amplitude and duration of the force generated by the quadriceps muscle contraction were compared in the WT, LV.*Mpz-GJB1*-treated, and LV.*Mpz-Egfp*-treated mice.

Ex Vivo Sciatic Nerve CV. For ex vivo measurement of nerve CV, isolated sciatic nerves from LV.*Mpz-GJB1*- and LV.*Mpz-Egfp*-treated mice were placed in a Petri dish containing well-oxygenated saline solution containing 136 mM NaCl, 11 mM glucose, 4.7 mM KCl, 2.4 mM $CaCl_2$, 1.1 mM $MgCl_2$, 1 mM $NaHCO_3$, and 10 mM Hepes, pH 7.2. All experiments were performed at a constant temperature of 25 ± 1 °C. The mice were euthanized according to institutionally approved protocols. A 24-carat gold stimulating hook electrode was placed on the proximal end of the nerve, and a 24-carat gold recording hook electrode was placed on two different sides of the nerve. The nerve was stimulated using a constant-current stimulator (DS3; Digitimer) at 1 mA and a 20-μs pulse duration. The CAP was recorded from the different sides across the nerve (recording points R1 and R2 for the middle and distal regions, respectively), as indicated in Fig. 3*D*, and the CV was calculated according to the following formula: $v = ds/dt$, where v is CV, ds is the distance between the two recording points R1 and R2, and dt is the time difference between the two points. CV was also measured in nerves of WT mice to validate our methodology.

Immunohistochemistry. For immunostaining, mice were anesthetized with avertin according to institutionally approved protocols, and then transcardially perfused with normal saline followed by fresh 4% paraformaldehyde in 0.1 M buffer PB. The lumbar-sacral spinal cord with all roots attached were dissected, along with L2–L6 DRG; the bilateral sciatic nerves, divided into proximal, middle, and distal sections; the bilateral femoral nerves; and the quadriceps muscle (*SI Appendix*, Fig. S2). Intracranial trigeminal nerves were dissected as well. All tissues were frozen for cryosections. The sciatic and femoral nerves were isolated and teased into fibers under a stereoscope. Teased fibers or sections were permeabilized in cold acetone and incubated at room temperature with a blocking solution of 5% BSA containing 0.5% Triton-X for 1 h. Primary antibodies were mouse monoclonal antibody against Cx32 (1:50; Invitrogen), Kv1.1 (1:500; Upstate Biotechnology), CD3 (1:100; Abcam), myelin basic protein (1:500; Abcam), RT-97 (1:1,000; Developmental Studies Hybridoma Bank), GFAP (1:400; Sigma-Aldrich), Glut-1 (1:200; Abcam), Vimentin (1:50; Millipore); rabbit antisera against EGFP (1:2,000; Invitrogen), Cx32 (1:50; Invitrogen), CD3 (1:100, Abcam), Caspr2 (1:100; Sigma-Aldrich), fibronectin (1:500; Dako), and fibrinogen (1:100; Dako); rat anti-CD68 (1:50; Serotec) and anti-CD45 (1:100, Abcam); and goat anti-EGFP (1:100; Santa Cruz Biotechnology), all diluted in blocking solution and incubated overnight at 4 °C.

Slides were then washed in PBS and incubated with fluorescein- and rhodamine-conjugated donkey, goat, and rabbit cross-affinity purified secondary antibodies (Jackson ImmunoResearch, diluted 1:500; Invitrogen, 1:2,000; Abcam, 1:700) for 1 h at room temperature. Cell nuclei were visualized with DAPI. Slides were mounted with fluorescent mounting medium and images photographed under a fluorescence microscope with a digital camera using Axiovision software (Carl Zeiss MicroImaging).

Quantification of EGFP expression was performed at 2, 8, and 16 wk postinjection in six sections (roots) or six teased fiber preparations (peripheral nerves) per mouse, in three mice per time point. Total numbers, as well as EGFP$^+$ Schwann cells, were counted to obtain the percentage of Schwann cells expressing EGFP (*SI Appendix*, Table S1). Statistical analysis was performed comparing the expression rates at different time points using one-way ANOVA and Tukey's posttest using GraphPad InStat.

Immunoblot Analysis. Fresh sciatic and femoral nerves and lumbar spinal roots were collected at 4–6 wk postinjection and lysed in ice-cold RIPA buffer (10 mM sodium phosphate, pH 7.0, 150 mM NaCl, 2 mM EDTA, 50 mM sodium fluoride, 1% Nonidet P-40, 1% sodium deoxycholate, and 0.1% SDS) containing a mixture of protease inhibitors (Roche). Proteins (150 μg) from the lysates were fractionated by 12% SDS/PAGE and then transferred to a Hybond-C Extra membrane (GE Healthcare Life Sciences) using a semidry transfer unit. Nonspecific sites on the membrane were blocked with 5%

Kagiava et al.

www.manaraa.com

nonfat milk in PBS with Tween 20 (PBST) for 1 h at room temperature. Immunoblots were incubated with rabbit antisera against EGFP (1:1,000; Abcam) or Cx32 (clone 918, 1:3,000) (45) and mouse β-tubulin (1:4,000; Developmental Studies Hybridoma Bank) or GAPDH (1:4,000; Santa Cruz Biotechnology) at 4 °C overnight. After washing, the immunoblots were incubated with an anti-mouse or anti-rabbit HRP-conjugated secondary antiserum (Jackson ImmunoResearch, diluted 1:3,000) in 5% milk–PBST for 1 h. The bound antibody was visualized by an enhanced chemiluminescence system (GE Healthcare Life Sciences).

RT-PCR. Snap-frozen sciatic nerves from intrathecally injected Cx32 KO and WT mice were collected at 4–6 wk postinjection. RNA was isolated with the Qiagen RNeasy Lipid Tissue Mini Kit following the manufacturer's protocol. After DNase treatment, RNA was quantified by spectrophotometry. Then 0.5 μg of RNA was used to synthesize cDNA using Taqman reverse-transcription reagents (Applied Biosystems). cDNA was amplified using Cx32-F (5′-TGAGGCAGGAT-GAACTGGACAGGT-3′) and Cx32-R (5′-CACGAAGCAGTCCACTGT-3′) primers. cDNA was then digested with MscI or HhaI, as well as with both enzymes, as described previously (14). MscI cuts the human cDNA into two fragments (280 and 273 bp), and HhaI cuts the mouse cDNA product into two fragments (230 and 323 bp). Digestions were run on 1.5% agarose gel to estimate the relative levels of exogenous/human and endogenous/mouse mRNAs.

Morphometric Analysis of Lumbar Roots and Peripheral Nerve Pathology. Mice (n = 8 per treatment group) were transcardially perfused with 2.5% glutaraldehyde in 0.1 M buffer PB. The lumbar spinal cord with multiple spinal roots attached, as well as the femoral and sciatic nerves, were dissected and fixed overnight at 4 °C, then osmicated, dehydrated, and embedded in araldite resin. Transverse semithin sections (1 μm) of the lumbar spinal cord with roots and the middle portion of the femoral motor and sciatic nerves were obtained and stained with alkaline toluidine blue. Sections were visualized with 10×, 20×, and 40× objective lenses and captured with a Zeiss AxioCam HR camera. Images of whole root or transverse nerve sections were obtained at 100–200× final magnification, and a series of partially overlapping fields covering the cross-sectional area of the nerve were captured at 400× final magnification. These images were used to examine the degree of abnormal myelination in both groups as described previously (8, 14, 15). In brief, all demyelinated, remyelinated, and normally myelinated axons were counted using the following criteria: axons larger than 1 μm without a myelin sheath were considered demyelinated, axons with

myelin sheaths <10% of the axonal diameter and/or axons surrounded by "onion bulbs" (i.e., circumferentially arranged Schwann cell processes and extracellular matrix) were considered remyelinated, and other myelinated axons were considered normally myelinated.

In addition, the number of foamy macrophages present in the entire cross-section of each root or nerve were counted, as an indication of inflammation. Macrophages were identified in semithin sections at 400× magnification as cells laden with myelin debris, devoid of a basement membrane, and extending small, microvilli-like processes, as described previously (16, 46). The macrophage count was calculated as the ratio per 1,000 myelinated fibers, to account for size differences between different roots and nerves.

For quantification of inflammatory cells in treated and mock-treated mice, longitudinal lumbar spinal cord fixed-frozen sections with attached roots, as well as longitudinal sciatic nerve sections, were immunostained with macrophage (CD68), lymphocyte (CD3), and leukocyte (CD45) markers, and the number of positive cells was determined in at least three different sections per tissue in four mice per group. Counts were expressed as a ratio of inflammatory cells per total cell number (by counting all DAPI-stained nuclei) in each section, to account for size differences. All pathological analyses were performed blinded to the treatment condition in each mouse.

Statistics. Behavioral and electrophysiological analysis data of the mock-treated and fully treated mice were compared using the unpaired two-sided t test with Graphad Instat3 software. In the morphometric analysis using semithin sections, the proportion of abnormally myelinated fibers and the number of macrophages in lumbar roots and femoral and sciatic nerves in the mock-treated and fully treated mice were compared using the Mann–Whitney U test (significance level, $P < 0.05$) with Microsoft Excel and Minitab 15 statistical software. Inflammatory cell counts in immunostained tissues were compared using the unpaired two-sided t test.

1. Saporta MA, Shy ME (2013) Inherited peripheral neuropathies. *Neurol Clin* 31(2):597–619.
2. Baets J, De Jonghe P, Timmerman V (2014) Recent advances in Charcot-Marie-Tooth disease. *Curr Opin Neurol* 27(5):532–540.
3. Harel T, Lupski JR (2014) Charcot-Marie-Tooth disease and pathways to molecular-based therapies. *Clin Genet* 86(5):422–431.
4. Bouhy D, Timmerman V (2013) Animal models and therapeutic prospects for Charcot-Marie-Tooth disease. *Ann Neurol* 74(3):391–396.
5. Homs J, et al. (2011) Schwann cell targeting via intrasciatic injection of AAV8 as gene therapy strategy for peripheral nerve regeneration. *Gene Ther* 18(6):622–630.
6. Federici T, et al. (2009) Comparative analysis of HIV-1–based lentiviral vectors bearing lyssavirus glycoproteins for neuronal gene transfer. *Genet Vaccines Ther* 7:1.
7. Gonzalez S, Fernando RN, Perrin-Tricaud C, Tricaud N (2014) In vivo introduction of transgenes into mouse sciatic nerve cells in situ using viral vectors. *Nat Protoc* 9(5):1160–1169.
8. Sargiannidou I, et al. (2015) Intraneural GJB1 gene delivery improves nerve pathology in a model of X-linked Charcot-Marie-Tooth disease. *Ann Neurol* 78(2):303–316.
9. Scherer SS, et al. (2005) Transgenic expression of human connexin32 in myelinating Schwann cells prevents demyelination in connexin32-null mice. *J Neurosci* 25(6):1550–1559.
10. Anzini P, et al. (1997) Structural abnormalities and deficient maintenance of peripheral nerve myelin in mice lacking the gap junction protein connexin 32. *J Neurosci* 17(12):4545–4551.
11. Scherer SS, et al. (1998) Connexin32-null mice develop demyelinating peripheral neuropathy. *Glia* 24(1):8–20.
12. Kleopa KA, Scherer SS (2006) Molecular genetics of X-linked Charcot-Marie-Tooth disease. *Neuromolecular Med* 8(1-2):107–122.
13. Scherer SS, et al. (1995) Connexin32 is a myelin-related protein in the PNS and CNS. *J Neurosci* 15(12):8281–8294.
14. Sargiannidou I, et al. (2009) Connexin32 mutations cause loss of function in Schwann cells and oligodendrocytes leading to PNS and CNS myelination defects. *J Neurosci* 29(15):4736–4749.
15. Vavlitou N, et al. (2010) Axonal pathology precedes demyelination in a mouse model of X-linked demyelinating/type I Charcot-Marie-Tooth neuropathy. *J Neuropathol Exp Neurol* 69(9):945–958.
16. Kobsar I, et al. (2003) Preserved myelin integrity and reduced axonopathy in connexin32-deficient mice lacking the recombination activating gene-1. *Brain* 126(Pt 4):804–813.

17. Wang Ip C, et al. (2006) Role of immune cells in animal models for inherited peripheral neuropathies. *Neuromolecular Med* 8(1-2):175–190.
18. Haller FR, Low FN (1971) The fine structure of the peripheral nerve root sheath in the subarachnoid space in the rat and other laboratory animals. *Am J Anat* 131(1):1–19.
19. McCabe JS, Low FN (1969) The subarachnoid angle: An area of transition in peripheral nerve. *Anat Rec* 164(1):15–33.
20. Mellick R, Cavanagh JB (1967) Longitudinal movement of radioiodinated albumin within extravascular spaces of peripheral nerves following three systems of experimental trauma. *J Neurol Neurosurg Psychiatry* 30(5):458–463.
21. Low PA (1985) Endoneurial potassium is increased and enhances spontaneous activity in regenerating mammalian nerve fibers: Implications for neuropathic positive symptoms. *Muscle Nerve* 8(1):27–33.
22. Mizisin AP, Weerasuriya A (2011) Homeostatic regulation of the endoneurial microenvironment during development, aging and in response to trauma, disease and toxic insult. *Acta Neuropathol* 121(3):291–312.
23. Vulchanova L, et al. (2010) Differential adeno-associated virus mediated gene transfer to sensory neurons following intrathecal delivery by direct lumbar puncture. *Mol Pain* 6:31.
24. Glatzel M, et al. (2000) Adenoviral and adeno-associated viral transfer of genes to the peripheral nervous system. *Proc Natl Acad Sci USA* 97(1):442–447.
25. Beutler AS, Banck MS, Walsh CE, Milligan ED (2005) Intrathecal gene transfer by adeno-associated virus for pain. *Curr Opin Mol Ther* 7(5):431–439.
26. Jacques SJ, et al. (2012) AAV8(gfp) preferentially targets large diameter dorsal root ganglion neurones after both intra-dorsal root ganglion and intrathecal injection. *Mol Cell Neurosci* 49(4):464–474.
27. Bevan AK, et al. (2011) Systemic gene delivery in large species for targeting spinal cord, brain, and peripheral tissues for pediatric disorders. *Mol Ther* 19(11):1971–1980.
28. Fedorova E, Battini L, Prakash-Cheng A, Marras D, Gusella GL (2006) Lentiviral gene delivery to CNS by spinal intrathecal administration to neonatal mice. *J Gene Med* 8(4):414–424.
29. Dengler EC, et al. (2014) Improvement of spinal non-viral IL-10 gene delivery by D-mannose as a transgene adjuvant to control chronic neuropathic pain. *J Neuroinflammation* 11:92.
30. Luo MC, et al. (2005) An efficient intrathecal delivery of small interfering RNA to the spinal cord and peripheral neurons. *Mol Pain* 1:29.
31. Song Z, Zou W, Liu C, Guo Q (2010) Gene knockdown with lentiviral vector-mediated intrathecal RNA interference of protein kinase C gamma reverses chronic morphine tolerance in rats. *J Gene Med* 12(11):873–880.
32. Lepore AC, Bakshi A, Swanger SA, Rao MS, Fischer I (2005) Neural precursor cells can be delivered into the injured cervical spinal cord by intrathecal injection at the lumbar cord. *Brain Res* 1045(1-2):206–216.

www.manaraa.com

33. Watson G, et al. (2006) Intrathecal administration of AAV vectors for the treatment of lysosomal storage in the brains of MPS I mice. *Gene Ther* 13(11):917–925.

34. Duque SI, et al. (2015) A large animal model of spinal muscular atrophy and correction of phenotype. *Ann Neurol* 77(3):399–414.

35. Kleopa KA (2011) The role of gap junctions in Charcot-Marie-Tooth disease. *J Neurosci* 31(49):17753–17760.

36. Shy ME, et al. (2007) CMT1X phenotypes represent loss of GJB1 gene function. *Neurology* 68(11):849–855.

37. Lattanzi A, et al. (2014) Therapeutic benefit of lentiviral-mediated neonatal intracerebral gene therapy in a mouse model of globoid cell leukodystrophy. *Hum Mol Genet* 23(12):3250–3268.

38. Biffi A, et al. (2011) Lentiviral vector common integration sites in preclinical models and a clinical trial reflect a benign integration bias and not oncogenic selection. *Blood* 117(20):5332–5339.

39. Biffi A, et al. (2013) Lentiviral hematopoietic stem cell gene therapy benefits metachromatic leukodystrophy. *Science* 341(6148):1233158.

40. Christodoulou I, et al. (2016) Measurement of lentiviral vector titre and copy number by cross-species duplex quantitative PCR. *Gene Ther* 23(1):113–118.

41. Geraerts M, Willems S, Baekelandt V, Debyser Z, Gijsbers R (2006) Comparison of lentiviral vector titration methods. *BMC Biotechnol* 6:34.

42. Savvaki M, et al. (2010) The expression of TAG-1 in glial cells is sufficient for the formation of the juxtaparanodal complex and the phenotypic rescue of tag-1 homozygous mutants in the CNS. *J Neurosci* 30(42):13943–13954.

43. Britt JM, et al. (2010) Polyethylene glycol rapidly restores axonal integrity and improves the rate of motor behavior recovery after sciatic nerve crush injury. *J Neurophysiol* 104(2):695–703.

44. Pratt SJ, Lovering RM (2014) A stepwise procedure to test contractility and susceptibility to injury for the rodent quadriceps muscle. *J Biol Methods* 1(2):e8.

45. Ahn M, et al. (2008) Cx29 and Cx32, two connexins expressed by myelinating glia, do not interact and are functionally distinct. *J Neurosci Res* 86(5):992–1006.

46. Groh J, et al. (2010) Attenuation of MCP-1/CCL2 expression ameliorates neuropathy in a mouse model for Charcot-Marie-Tooth 1X. *Hum Mol Genet* 19(18):3530–3543.